Original Article

The conversion of ammonium uranate prepared via sol-gel synthesis into uranium oxides

Christian Schreinemachers [a, b, *], Gregory Leinders [a], Giuseppe Modolo [c], Marc Verwerft [a], Koen Binnemans [b], Thomas Cardinaels [a, b]

[a] Belgian Nuclear Research Centre (SCK•CEN), Institute for Nuclear Materials Science, Boeretang 200, B-2400 Mol, Belgium
[b] KU Leuven, Department of Chemistry, Celestijnenlaan 200F, P.O. Box 2404, B-3001 Heverlee, Belgium
[c] Forschungszentrum Jülich GmbH, Institute of Energy and Climate Research (IEK), IEK-6: Nuclear Waste Management and Reactor Safety, 52425 Jülich, Germany

A B S T R A C T

A combination of simultaneous thermal analysis, evolved gas analysis and non-ambient XRD techniques was used to characterise and investigate the conversion reactions of ammonium uranates into uranium oxides. Two solid phases of the ternary system $NH_3 - UO_3 - H_2O$ were synthesised under specified conditions. Microspheres prepared by the sol-gel method via internal gelation were identified as $3UO_3 \cdot 2NH_3 \cdot 4H_2O$, whereas the product of a typical ammonium diuranate precipitation reaction was associated to the composition $3UO_3 \cdot NH_3 \cdot 5H_2O$. The thermal decomposition profile of both compounds in air feature distinct reaction steps towards the conversion to U_3O_8, owing to the successive release of water and ammonia molecules. Both compounds are converted into α-U_3O_8 above 550 °C, but the crystallographic transition occurs differently. In compound $3UO_3 \cdot NH_3 \cdot 5H_2O$ (ADU) the transformation occurs via the crystalline β-UO_3 phase, whereas in compound $3UO_3 \cdot 2NH_3 \cdot 4H_2O$ (microspheres) an amorphous UO_3 intermediate was observed. The new insights obtained on these uranate systems improve the information base for designing and synthesising minor actinide-containing target materials in future applications.
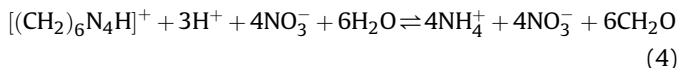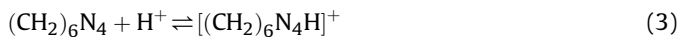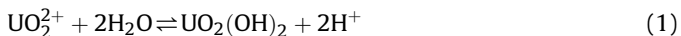
1. Introduction

Conventional powder processing is today the reference process for ceramic nuclear fuel production (UO_2 and $(U, Pu)O_2$). Since more than six decades, however, sol-gel processes have been explored to avoid handling of fine powder and to facilitate automation for the production of nuclear fuel particles [1–6]. Common sol-gel methods are the routes via internal- and external gelation. Both methods are based on the precipitation of a metal nitrate solution by ammonia into a metal hydroxide, but differ amongst others in the source of ammonia. In the external gelation process, the sol is dispersed into droplets which are given into an ammonia solution, whereas in the internal gelation (IG) process, reagents are added to the sol which decompose thermally and release ammonia within droplets of the sol. The resulting particles are

thermally treated and can directly be used as particle fuel [7] or compressed into the commonly used fuel pellets [8]. The IG process offers the opportunity to handle a mixture of different metals resulting in a homogeneous precipitate. MOX particles [9] as well as U/Pu nitride particles [10] have been prepared via IG and it might be a promising strategy to produce americium-containing transmutation fuel [11]. The production of neodymium-doped UO_2 particles (Nd as Am surrogate) has been demonstrated as well [12].

Hexamethylenetetramine (HMTA, $(CH_2)_6N_4$) and urea ($CO(NH_2)_2$) are used as gelation agents in the IG process. Vaidya et al. [13] studied the influence of these agents on the gelation process for different uranium concentrations in the sol. The chemistry of the IG process was described by Collins et al. [14] as a hydrolysis reaction (1) resulting in a precipitate with $UO_3 \cdot 2H_2O$ stoichiometry (reaction (2)). The acid formed during hydrolysis is consumed during the protonation and decomposition of HMTA, as shown in reactions (3) and (4).

$$UO_2^{2+} + 2H_2O \rightleftharpoons UO_2(OH)_2 + 2H^+ \tag{1}$$

$$UO_2(OH)_2 \cdot H_2O \rightleftharpoons UO_3 \cdot 2H_2O \downarrow \tag{2}$$

$$(CH_2)_6N_4 + H^+ \rightleftharpoons [(CH_2)_6N_4H]^+ \tag{3}$$

$$[(CH_2)_6N_4H]^+ + 3H^+ + 4NO_3^- + 6H_2O \rightleftharpoons 4NH_4^+ + 4NO_3^- + 6CH_2O \tag{4}$$

During the IG process ammonium cations are generated (reaction (4)) causing a pH increase in the sol. This results in an ammonium diuranate (ADU) like precipitate [15,16], generally described as $xUO_3 \cdot yNH_3 \cdot zH_2O$, with $x = \frac{y+z}{2}$ [17], which is in contradiction to the precipitate formed in reaction (2). Moreover, the gelled particles are contacted with ammonia solution during the post gelation treatment to ensure completion of the gelation reaction, possibly leading to gels containing NH_3.

In this study we characterise the gel via X-ray diffraction (XRD) and investigate its thermal decomposition in air by simultaneous thermogravimetric analyses (STA) up to a temperature of 1300 °C. Changes in crystallographic structure are followed by in-situ high-temperature X-ray diffraction (HT-XRD) between room temperature and 650 °C. A comparison with ADU powder prepared via addition of ammonia solution to uranyl nitrate solution (UNS) is carried out and the results are discussed with literature [18–20]. The conversion reactions into uranium oxides, produced from different precursor materials are relevant for the fabrication of advanced nuclear fuels and minor actinide-containing target materials, as well as in the context of nuclear forensic investigations [18].

2. Experimental

2.1. Chemicals

UO_{2+x} ($x = 0.06(1)$) originates from a stock provided by AREVA and is depleted in $^{235}_{92}U$ (0.3 g/100 g U). Impurities were analysed and have been found to be < 0.01 %. Nitric acid ($w(HNO_3) = 70 \%$; ≥ 99.999 %; trace metals basis) was purchased from Aldrich. Ammonia solution ($w(NH_3) = 28 \%$–30 %; ACS reagent®), urea (pellets; ≥ 99.5 %; ReagentPlus®) and HMTA (≥ 99.0 %; ACS reagent®) were purchased from Sigma-Aldrich, while silicone oil (47 V 100) and petroleum benzine (40 °C to 60 °C boiling range; SupraSolv®) originated from VWR.

2.2. ADU powder preparation

A uranyl nitrate solution (UNS) with $c(U) = 1.8 \, mol \, L^{-1}$ was prepared by dissolving UO_{2+x} in stoichiometric amounts of HNO_3. Ammonium diuranate (ADU) was precipitated from the UNS via addition of ammonia solution while stirring. The precipitate was separated using a Büchner funnel. The cake was washed with ultrapure water and the product was dried for 24 h at 50 °C and ambient pressure. Afterwards, the pressure was stepwise reduced to 50 mbar and the product was kept under those conditions for another 24 h.

2.3. Particle synthesis by internal gelation

Uranium-containing microspheres were prepared via IG using an acid-deficient uranyl nitrate (ADUN) solution as precursor. The ADUN solution ($c(U) = 2.6 \, mol \, L^{-1}$, pH = 1.7, $\rho = 1.85 \, g \, cm^{-3}$, $\frac{c(NO_3^-)}{c(U)} = 1.56$) was prepared by dissolving β-UO_3 in UNS as

described by Haas et al. [21]. The β-UO_3 was synthesised by thermal decomposition of ADU according to the method described by Grenthe et al. [22] (pp. 341–342). A heating rate of 5 °C min^{-1} was applied to reach 450 °C and this temperature was kept for 1 h, the thermal treatment was carried out in air at ambient pressure.

The amounts of the gelation agents in the sol are defined by their molar amount over the molar metal amount (R). For a uranium concentration of 1.3 mol L^{-1} in the sol, Vaidya et al. [13] determined a concentration ratio $R = 1.2$ for both gelation agents (HMTA and urea) to form a single phase gel at 50 °C to 70 °C.

The ADUN solution (2.0 mL) was stirred in an ice bath and 2.0 mL of a pre-cooled solution containing HMTA (3.1 mol L^{-1}) and urea (3.1 mol L^{-1}) was added, leading to $c(U) = 1.3 \, mol \, L^{-1}$ and $R = 1.2$ for both gelation agents. The sol was dropped manually into a double-walled glass column filled with silicone oil ($T = 90$ °C) by the use of a syringe and a hollow needle (diameter = 0.45 mm). When the sol was added, the set-up was cooled to 40 °C and the gelled droplets were removed from the column. They were washed 3 times with 50 mL petroleum benzine and stored in 50 mL of ammonia solution ($w(NH_3) = 12.5 \%$). After ageing for 24 h, the particles were washed twice with 50 mL ammonia solution ($w(NH_3) = 12.5 \%$) and dried for 24 h at room temperature. Finally, the products were dried at 90 °C and a pressure of 250 mbar for 24 h.

Spherical particles were achieved and 1.7 g of dried particles, with an average particle mass of 3.7(1) mg, were produced. During the ageing and washing of the gelled droplets with ammonia solution, uranium erosion was observed. Similar observations were made by Hunt et al. [23] for gels fabricated with different sol compositions but comparable temperatures.

2.4. Determination of U and NO_3^- concentration

Uranium concentrations of the UNS and the ADUN solution were determined via inductive coupled plasma mass spectrometry (ICP-MS). An ELEMENT 2 system (Thermo Scientific) was calibrated with 1 ppb, 2 ppb, 5 ppb, 10 ppb and 20 ppb U solutions, prepared from a 1000 ppm U single element standard (SPEX, CertiPrep) diluted with a matrix consisting of ultrapure water and HNO_3 (2 % $\frac{V}{V}$). A dilution factor of $1 : 10^8$ was applied to the sample solutions.

The molar NO_3^- concentration was estimated to calculate the $\frac{c(NO_3^-)}{c(U)}$ ratio of the ADUN solution, using a relation between the molar U concentration, the density and the NO_3^- concentration as described by Haas et al. [3]. The density was determined by pipetting ten times 1.0 mL solution into a beaker and measuring the individual masses on an analytical balance (Mettler-Toledo AT201).

2.5. X-ray powder diffraction (XRD)

XRD analyses were carried out using a PANanalytical X'Pert Pro diffractometer. The device utilises a Bragg–Brentano parafocusing geometry in a $\theta - \theta$ configuration. A sintered, high purity silicone disc was used for zero point calibration. Weekly validations were performed on a sintered alumina disc (NIST Standard Reference Material 1976b). Lattice parameter refinement of silicone was done to asses the instrument bias, which was found to be smaller than 2×10^{-5} relative (2σ). A copper LFF X-ray tube ($K\alpha_1 = 1.5405929$ Å [24]) was used as radiation source. The measurement of high-quality diffractograms with low axial divergence was ensured by a combination of a fixed divergence slit, 0.02 rad soller slits and a copper beam mask in the incident beam path. The diffracted beam path was foreseen with a nickel filter and detection was done with a position-sensitive detector (PANalytical X'Celerator).

A suspension of sample material in ethanol was dropped on a zero background silicone single crystal holder. After evaporation of

the ethanol, the specimen was mounted into the device and dif-fractograms were recorded from 10° to 90° 2θ with a step size of 0.017° 2θ.

HT-XRD investigations were carried out using the same diffractometer, equipped with an *Edmund Bühler* high-temperature chamber (Hochtemperaturkammer HDK 2.4). A suspension of the sample in ethanol was dropped on a Pt/Rh heating strip. After the ethanol was evaporated, the high-temperature chamber was flushed with 250 mL min^{-1} synthetic air and the diffractogram was recorded between 10° and 90° 2θ with a step size of 0.033° 2θ. The initial XRD pattern was recorded at room temperature, then a heating rate of 2 °C min^{-1} was applied. The heating process was intermitted at 150 °C, 250 °C, 350 °C, 450 °C, 550 °C, 600 °C and 650 °C to perform a scan.

Lattice parameters were determined using the *Rietveld* method and the *Pawley* fit option of the software package HighScore Plus by PANalaytical (Version 4.8).

2.6. Thermogravimetric analyses (TGA) and differential scanning calorimetry (TG-DSC)

TGA and TG-DSC analyses were performed using a *NETZSCH STA 449 F1 Jupiter* thermobalance. The device is linked to a QMS 403 C Aëolos evolved gas analysis-mass spectrometer (EGA-MS). The absolute uncertainty on mass readout including drift and noise of the apparatus was measured to be ± 0.03 mg (2σ). TGA mea-surements were carried out in alumina crucibles with a heating rate of 2 °C min^{-1} and a sample mass of about 200 mg, while a sample mass of about 35 mg, Pt/Rh crucibles and a heating rate of 10 °C min^{-1} were used for the TG-DSC measurements. The particles were ground in a mortar prior to the analyses.

In both modes, the set-up was evacuated to ≤ 0.15 mbar, then synthetic air was introduced into the furnace and the measurement was carried out purging the system with 80 mL min^{-1} synthetic air and the balance compartment with 20 mL min^{-1} argon as protec-tive gas. The temperature program contained isothermal segments of 40 °C at the beginning (30 min) and the end (60 min) of each analysis. The mass present at the end of the initial equilibration plateau was considered as initial *in-situ* mass.

The tare mass of the crucible, as well as the mass of the crucible containing the sample was measured prior to and after the TG analysis (Mettler-Toledo AT201), having an uncertainty of ± 0.04 mg (2σ). The *ex-situ* masses were used to calculate absolute mass differences and quantify the losses occurred during the evacuation of the TG set-up.

3. Results

3.1. XRD analyses

XRD patterns of the dried gelation products measured in ambient mode and in HT configuration at room temperature are shown in Fig. 1. The data acquired in both modes are in good agreement to each other. In the pattern obtained in HT mode additional reflections caused by the Pt/Rh heating strip were observed (12.96°, 40.21° and 46.72°). An XRD measurement of the Pt/Rh heating strip without sample material is part of the dataset of this study [25], the observed reflections are in agreement to pattern published for a Pt/Rh phase [26].

The diffractograms obtained for the IG particles are similar to those of the ADU powder. However, there are slight variations in the data. The diffractograms measured for the ADU powder exhibit more reflections than those of the IG particles, the most emphas-ised ones occur at 2θ diffraction angles of 18.65° and 31.55° (boxes in Fig. 1). Additionally, less intense reflections were observed at
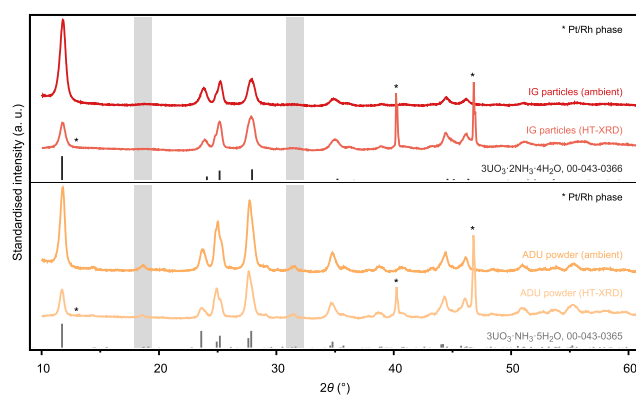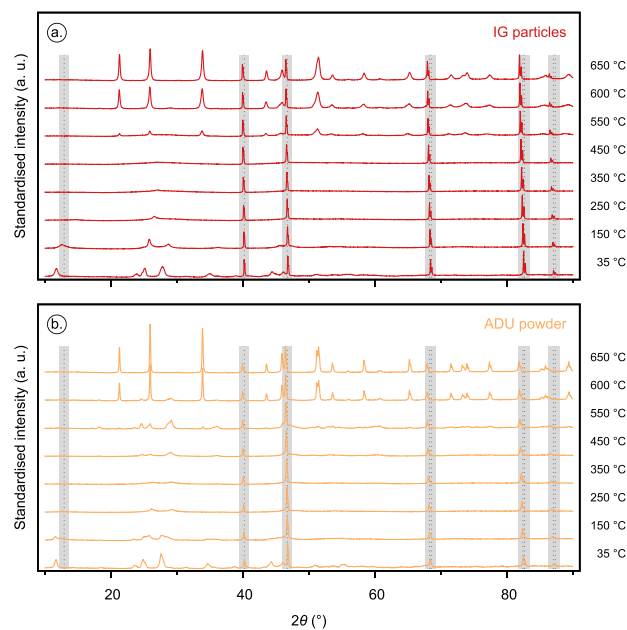

Fig. 1. X-ray diffraction patterns measured in ambient mode for the particles prepared by internal gelation (IG particles, top) and the ADU powder (bottom), as well as the data obtained at room temperature in HT mode and reference pattern taken from the PDF-2 database (00-043-0366 [27], 00-043-0365 [27]). The shaded regions mark the most emphasised differences between the patterns of both compounds.

14.40°, 29.20°, 38.80°, 40.75°, 43.24°, 48.45°, 50.97° and 55.35° for the ADU powder.

The HT-XRD data for the temperature region from 35 °C to 650 °C are presented in Fig. 2. They show the Pt/Rh reflections recognised in Fig. 1 and additional Pt/Rh reflections at 68.28°, 82.40° and 86.97° [26]. Between 250 °C and 550 °C an amorphous phase is present in both compounds. For the ADU powder, β-UO_3 reflections were clearly recognised at 450 °C and 550 °C. In contrast, these reflections could not be identified in the corre-sponding diffractograms of the IG particles. At 550 °C an additional set of reflections indicate the transition to α-U_3O_8 for both com-pounds. It is almost completed at 600 °C, traces of the β-UO_3 are still visible in the pattern (29.15°) of the ADU powder. The scan taken at 650 °C shows that both materials are fully converted to α-U_3O_8.

The XRD pattern recorded at ≥ 450 °C were selected for full

Fig. 2. X-ray diffraction pattern obtained during the HT-XRD measurements of the IG particles (a.) and the ADU powder (b.) for the temperature range between 35 °C and 650 °C, as well as reflections of Pt/Rh (dashed vertical lines in the shaded ranges).

pattern refinement. Rietveld fits were applied using the β-UO_3 (ICSD: 14314 [27]) and α-U_3O_8 phase (ICSD: 28137 [28]), while the Pt/Rh phase (ICSD: 40356 [26]) was considered by a Pawley fit, to account for the non ideal diffraction properties of this phase. Phases with a scale factor of ≤ 1 % were not taken into account for the refinement. The determined UO_3 and α-U_3O_8 contents, as well as the *goodness of fit* (GOF) and *weighted-profile R-factor* (R_{wp}) of the refinements are listed in Table 1.

The β-UO_3 phase was identified for the ADU powder already at 450 °C, while for the IG particles mainly amorphous UO_3 was present and only traces of β-UO_3 were found at 600 °C. The β-UO_3 and α-U_3O_8 contents at 600 °C differ notably between the IG particles and the ADU powder (14.1 %, Table 1). The diffractograms of both samples at 650 °C (Fig. 3) are in good agreement with the α-U_3O_8 reference pattern and evidence the complete conversion into α-U_3O_8.

The lattice parameter a, b and c of α-U_3O_8 resulting from the refinements are shown as function of the temperature in Fig. 4a–c. The uncertainties on the lattice parameter were multiplied with the *goodness of fit* parameter of the individual refinements. Varying α-U_3O_8 lattice parameter were observed for the IG particle sample, while the values obtained for the ADU sample are quite constant within their uncertainty (Fig. 4a–c). The cell volume is presented in Fig. 4d. At 650 °C an identical cell volume was determined for both samples (Fig. 4d).

3.2. TG analyses

Since the HT-XRD measurements indicated the presence of a single α-U_3O_8 phase at 650 °C, the mass signal was normalised to this temperature. The resulting data series for the heat-up process are shown in Fig. 5 and reveal the initial *in-situ* masses listed in Table 2. To take also the mass differences that occurred during the evacuation of the set-up prior to the measurement into account, the initial *ex-situ* masses as described in the Experimental section were considered (Table 2). The mass differences between the initial *ex-situ* and initial *in-situ* mass (Table 2) correspond most likely to adsorbed water which is removed during the initial purging and evacuation steps.

The first significant mass loss recorded during the measurements should correspond to the removal of H_2O molecules from the compounds. For the IG particles this occurs up to 185 °C. The mass signal for the ADU powder reveals two steps (Fig. 5). The first step occurs up to 164 °C and the second step up to 222 °C. The EGA-MS results can not be fully de-convoluted to uniquely identify the release of H_2O and NH_3 molecules, therefore the following mass loss steps correspond to the removal of both, H_2O and NH_3. For the IG particles we observed a significant mass loss (428 °C), followed by a minor one (585 °C), while for the ADU powder two significant steps were recognised (369 °C and 567 °C). The details of those individual mass loss steps are examined in the Discussion section,
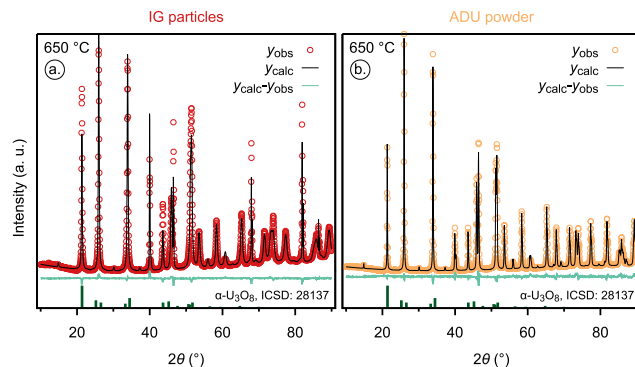

Fig. 3. XRD pattern observed during the HT-XRD measurements (y_{obs}), full pattern fit (y_{calc}) and difference between observed and calculated pattern ($y_{calc} - y_{obs}$) for the IG particles (a.) and the ADU powder (b.) at 650 °C, as well as reference pattern for α-U_3O_8 (ICSD: 28137 [28]).

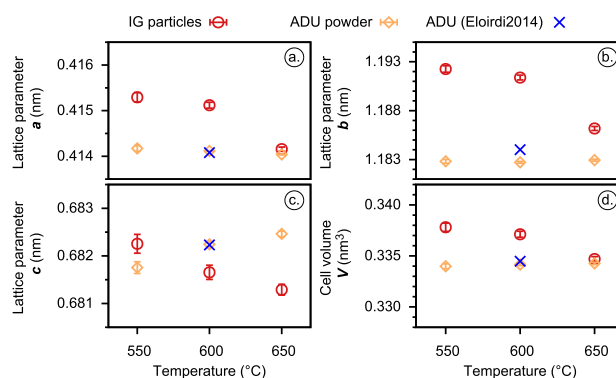**Fig. 4.** Lattice parameter a (a.), b (b.) and c (c.) of the α-U_3O_8 phase present in the IG particles and the ADU powder as function of the temperature, as well as the resulting cell volume (d.) and data published by Eloirdi et al. [18] for ADU at 600 °C.

taking also the EGA-MS and TG-DSC analyses into account.

The next mass loss can be assigned to the conversion of UO_3 to α-U_3O_8. Conversion temperatures were determined as 592 °C for the ADU powder and 610 °C for the IG particles. For the ADU powder, a more distinct transition occurring within a smaller temperature range was observed (Fig. 5, close-up). During this conversion, a mass difference of 2.07(5) % was found for the IG particles, while the mass difference for the ADU powder was 1.87(5) %. The theoretical mass difference for the conversion of UO_3 to U_3O_8 corresponds to 1.90 %.

A further gradual mass loss occurred during the heat-up process at temperatures above 800 °C, which may be interpreted as the formation of hypostoichiometric U_3O_8 as described by Grenthe et al. [22] (pp. 355–356).

Table 1
β-UO_3 and α-U_3O_8 contents determined via Rietveld refinement for the IG particles and the ADU powder, as well as the *goodness of fit* (GOF) and *weighted-profile R-factor* (R_{wp}) of the refinements.

	IG particles				ADU powder			
T / °C	$w(\beta$-$UO_3)$ / %	$w(\alpha$-$U_3O_8)$ / %	GOF / %	R_{wp} / %	$w(\beta$-$UO_3)$ / %	$w(\alpha$-$U_3O_8)$ / %	GOF / %	R_{wp} / %
450	a				100	0	3.8	5.8
550	a	b			92.7	7.3	3.6	5.6
600	9.8	90.2	7.1	10.8	23.9	76.1	3.7	5.7
650	0	100	7.0	10.7	0	100	4.1	6.4

a Amorphous UO_3 phase.
b Crystalline α-U_3O_8 phase (due to presence of amorphous UO_3 not quantified).
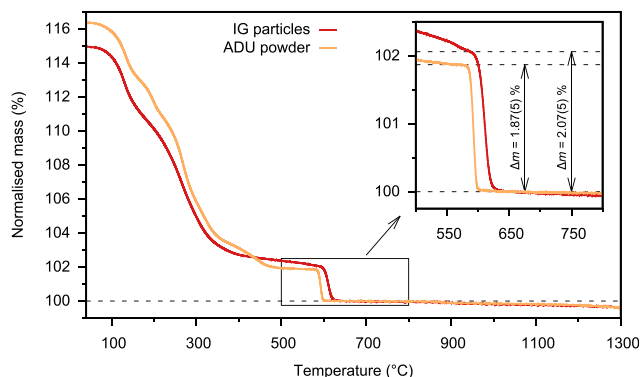
Fig. 5. TGA data obtained during the heating from room temperature to 1300 °C for the IG particles and the ADU powder (heating rate of 2 °C min^{-1}), masses normalised to $m(U_3O_8)$ at 650 °C.

Table 2

Initial *ex-situ* and *in-situ* masses for the IG particles and the ADU powder, as well as their differences (data normalised to $m(U_3O_8)$, 650 °C for TGA and 665 °C for TG-DSC measurements, uncertainties given with a confidence level of 2σ).

	IG particles		ADU powder	
	TGA / %	TG-DSC / %	TGA / %	TG-DSC / %
$m(\text{initial})_{ex-situ}$	123.31(2)	116.5(1)	117.48(2)	118.3(1)
$m(\text{initial})_{in-situ}$	114.96(3)	114.2(2)	116.37(3)	116.3(2)
Δm	8.35(4)	2.3(2)	1.11(4)	2.0(2)

The final *ex-situ* masses at room temperature were 99.65(2) % (IG particles) and 99.61(2) % (ADU powder), indicating U_3O_{8-x} as products with *x* values of 0.18(1) and 0.20(1) for the IG particles and the ADU powder, respectively.

The EGA-MS signals recorded up to 550 °C for $\frac{m}{z}$ equals 17 and 18 are shown in Fig. 6. A comparison of the results reveals a peak in the ADU data between 175 °C and 225 °C for the selected $\frac{m}{z}$ ratios, which is not present in the data recorded for the IG particles. This is in agreement with the additional reaction step in the ADU sample, observed in the TGA data. The data of the IG particles show a shoulder for the selected $\frac{m}{z}$ signals starting at approximately 330 °C, which could correspond to the release of NH_3 molecules not present in the ADU powder. Above 450 °C there was no emission of either H_2O or NH_3 observed.

The general trends observed in the TGA data could be confirmed via TG-DSC measurements. UO_3 to α-U_3O_8 conversion

temperatures were determined in the same way and have been found to be 625 °C for the IG particles and 609 °C for the ADU powder. Since the temperature difference between the TGA and TG-DSC measurements is about 15 °C, it was decided to standardise the TG-DSC data to the masses present at 665 °C. The temperature difference is caused by un-identical heating rates in TGA mode and TG-DSC mode (TG subsection, Experimental). The resulting data are summarised in Fig. 7.

The mass signal was treated like it was done for the TGA data. The initial *ex-situ* masses and initial *in-situ* masses, as well as their differences are listed in Table 2. Comparable differences were found, which indicate similar amounts of adsorbed water. The final masses were found to be 99.6(1) % (IG particles) and 99.7(1) % (ADU powder), leading to *x* values of 0.20(7) and 0.15(7) in U_3O_{8-x} for the IG particles and the ADU powder.

Due to the higher heating rate (10 °C min^{-1}) and smaller sample masses during the TG-DSC analysis, the masses and temperatures determined during the TGA analyses are more precise and the TG-DSC data were mainly used for interpretation of the DSC signal, which shows for both samples endothermic reactions indicating the release of H_2O below 275 °C (Fig. 7). Two peaks were observed for the IG particles (156 °C and 255 °C), while the data of the ADU powder exhibit three peaks (156 °C, 217 °C and 263 °C). This is a further indication for additional H_2O forms present in the ADU powder. We observed two exothermic peaks for the IG particles (313 °C and 385 °C) and one for the ADU powder (343 °C), they originate most likely from NH_3 release and agree to the EGA-MS investigations. Moreover, endothermic peaks were observed at 610 °C for the ADU powder and at 626 °C for the IG particles resulting from the conversion of UO_3 to α-U_3O_8. This peak is more intense for the ADU powder and not as broad as the one measured for the IG particles. Lastly, a minor endothermic peak was measured at 883 °C for the ADU powder.

The reaction enthalpies for the transition from UO_3 to α-U_3O_8 have been determined as 72(2) kJ mol^{-1} U_3O_8 for the IG particles (588 °C to 624 °C) and 81(2) kJ mol^{-1} U_3O_8 for the ADU powder (590 °C to 654 °C). Based on formation enthalpies for β-UO_3 and U_3O_8 published by Guéneau et al. [29] (tab. 13, p. 40), the theoretical reaction enthalpy is 86(10) kJ mol^{-1} U_3O_8.

4. Discussion

Cordfunke [17] demonstrated the existence of four solid phases in the system $NH_3 - UO_3 - H_2O$, which are listed in Table 3 and are possible candidates for our material. He observed that compounds IV and III are hygroscopic and unstable in contact with moist air.
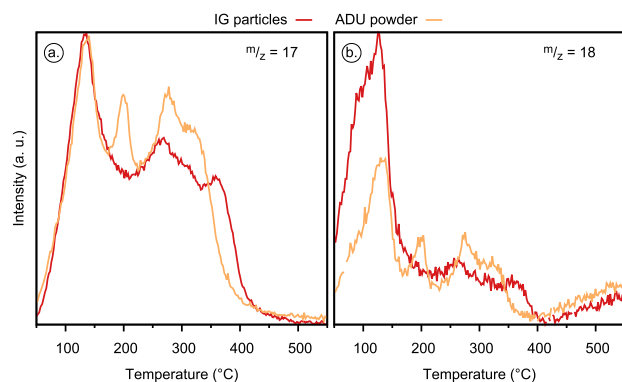
Fig. 6. EGA-MS data recorded for the signals of $\frac{m}{z} = 17$ (a.) and $\frac{m}{z} = 18$ (b.) during the TGA measurements between 50 °C and 550 °C for the IG particles and the ADU powder.
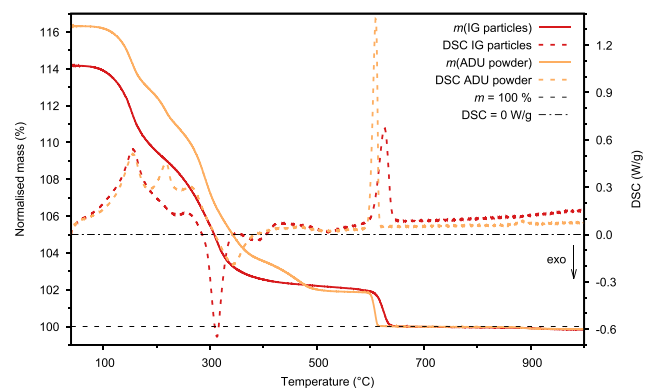
Fig. 7. TG-DSC data obtained during the heating from room temperature to 1000 °C for the IG particles and the ADU powder (heating rate of 10 °C min^{-1}), masses and DSC signals normalised to $m(U_3O_8)$ at 665 °C.

Table 3
Solid phases in the system $NH_3 - UO_3 - H_2O$[17], molar masses of the compounds (normalised to $n(UO_3)$) and theoretical mass differences originating from water $\Delta m(H_2O)$ and ammonia $\Delta m(NH_3)$, as well as the total mass difference for the decomposition to α-U_3O_8 $\Delta m(total)$. Mass differences normalised to $m(U_3O_8)$.

	Composition	M(composition)[a]	$\Delta m(H_2O)$[b]	$\Delta m(NH_3)$[b]	$\Delta m(total)$[b]
I	$UO_3 \cdot 2H_2O$	322.06 g mol^{-1}	−12.84 %		−14.74 %
II	$3UO_3 \cdot NH_3 \cdot 5H_2O$	321.73 g mol^{-1}	−10.70 %	−2.02 %	−14.62 %
III	$2UO_3 \cdot NH_3 \cdot 3H_2O$	321.57 g mol^{-1}	−9.63 %	−3.03 %	−14.56 %
IV	$3UO_3 \cdot 2NH_3 \cdot 4H_2O$	321.40 g mol^{-1}	−8.56 %	−4.04 %	−14.50 %

[a] M normalised to $n(UO_3)$ of composition.
[b] Δm normalised to $m(U_3O_8)$.

The ratio $\frac{n(NH_3)}{n(UO_3)}$ decreased as function of time and he explained this phenomenon by an exchange of NH_3 by H_2O in the lattice. Stable $\frac{n(NH_3)}{n(UO_3)}$ ratios were observed after 10 days, corresponding to compound III or compound II, respectively. Additionally, an increase in $\frac{n(H_2O)}{n(UO_3)}$ was observed, resulting in compounds with hyper-stoichiometric water contents. The stoichiometric compositions can be obtained by pumping the excess water off. In this way, compound IV is converted to compound III and compound III to compound II. For the latter, a constant $\frac{n(NH_3)}{n(UO_3)}$ ratio was observed, even at the presence of moist air. Consequently $3UO_3 \cdot NH_3 \cdot 5H_2O$ (compound II) is the only stable uranate in the ternary system $NH_3 - UO_3 - H_2O$.

4.1. Composition of dried material at room temperature

The room temperature diffractogram of the IG particles corresponds to $3UO_3 \cdot 2NH_3 \cdot 4H_2O$ (PDF-2: 00-043-0366 [27], compound IV), while the ADU powder has a better agreement with $3UO_3 \cdot NH_3 \cdot 5H_2O$ (PDF-2: 00-043-0365 [27], compound II). This proves the presence of an ADU like structure for the dried IG particles. The phase might not be stable, as described in the previous paragraph, and transforms via compound III into compound II, which was observed for the ADU powder. Moreover, varying differences in the initial *ex-situ* and initial *in-situ* masses for the two compounds were observed (Table 2), indicating a significantly higher quantity of loosely adsorbed water on the IG particles than on the ADU powder. The differences correspond to a content of 3.91(2) mol adsorbed water per 3 mol UO_3 for the IG particles and 0.52(2) mol per 3 mol β-UO_3 for the ADU powder.

Molar masses of the initial material were determined, taking the molar amounts of uranium based on $m(U_3O_8)$ into account. The initial *in-situ* masses lead to molar masses of M(IG particles) = 322.7(1) g mol^{-1} and M(ADU powder) = 326.7(1) g mol^{-1}, the molar masses are normalised to $n(UO_3)$. The theoretical molar masses for the compounds are listed in Table 3. Our samples show a higher molar mass than the expected one for the mentioned compositions, which indicates the presence of some excess H_2O and/or NH_3 in our material.

4.2. Decomposition: release of H_2O and NH_3

To better discuss the decomposition of the initial material in air Fig. 8 is added, showing the already introduced TGA results and the derivative of the corresponding TGA data (DTG), as well as the addressed mass differences up to 700 °C.

During the decomposition of the IG particles, we observed 3 mass loss steps up to the conversion to α-U_3O_8. The first step (Fig. 8b, $\Delta m_{IG, 1}$) is in agreement to the first peak occurring in the EGA-MS data (Fig. 6) and the DSC data (Fig. 7). A mass loss of 4.39(5) % was determined, which corresponds to a H_2O loss of 2.05(2) mol per 3 mol UO_3. The second step ($\Delta m_{IG, 2}$) can be related to a further dehydration reaction and an overlapping release of NH_3 (compare Fig. 6). The subsequent continuous minor mass loss ($\Delta m_{IG, 3}$) gives a
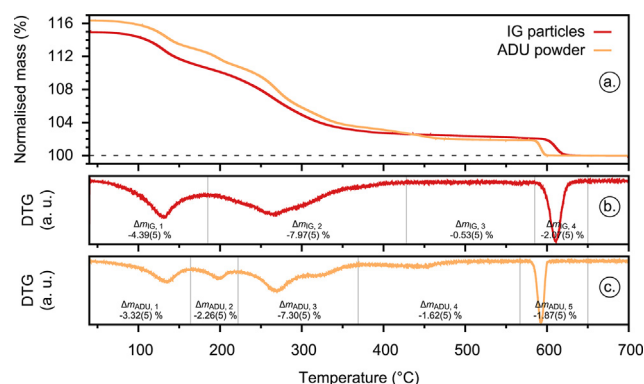
Fig. 8. TGA result for the IG particles and the ADU powder, as well as the corresponding DTG data and certain mass differences (heating rate of 2 °C min^{-1}, masses normalised to $m(U_3O_8)$ at 650 °C, uncertainties given with a confidence level of 2σ).

hint that no stable β-UO_3 is formed and was also taken into account to estimate H_2O and NH_3 contents. The XRD data (Fig. 1) implied a composition of 4 mol H_2O and 2 mol NH_3 per 3 mol UO_3 for the IG particles. A weighted molar mass based on the missing fraction of H_2O was used to estimate the missing fraction of both, H_2O and NH_3, which was found to be about 4.0 mol.
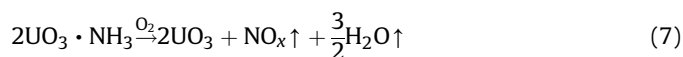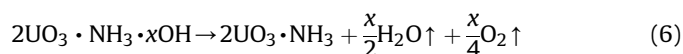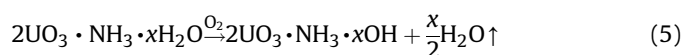
Burrell and Lee [30] investigated the decomposition of IG particles in vacuum using mass spectrometry and observed 3 peaks for $\frac{m}{z} = 18$. With an increasing heating rate the occurrence of those peaks shifted to a higher temperature. Lee and Stinton [31] performed a comparable study in different atmospheres. They applied a heating rate lower than Burrell and Lee [30], but equal to ours (2 °C min^{-1}). During the decomposition in air, a shift to higher temperatures was observed compared to the decomposition in vacuum. Additionally, the last two peaks occurred as one broad peak. We observed a temperature of about 125 °C for the first peak, which is comparable to the findings of Lee and Stinton [31], but our data allow identifying the last broad peak as two individual peaks (Fig. 6).

The decomposition of the ADU powder revealed an additional mass loss step up to the formation of α-U_3O_8. We assign the first two steps to the dehydration, leading to 1.55(2) mol H_2O per 3 mol UO_3 for $\Delta m_{ADU, 1}$ (Fig. 8c) and to 1.06(2) mol for $\Delta m_{ADU, 2}$. The following two steps ($\Delta m_{ADU, 3}$ and $\Delta m_{ADU, 4}$) were taken into account to estimate H_2O and NH_3 contents assuming an initial composition of 5 mol H_2O and 1 mol NH_3 per 3 mol UO_3. The missing fraction of H_2O and NH_3 was found to be about 4.2 mol. For $\Delta m_{ADU, 4}$, we can distinguish between a significant mass loss up to about 480 °C followed by a quite stable mass up to 567 °C indicating the formation of a stable β-UO_3 phase. The mass loss steps match well to the EGA-MS (Fig. 6) and DSC (Fig. 7) results for the ADU powder.
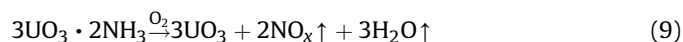
The mass loss $\Delta m_{ADU, 2}$ and the significant part of $\Delta m_{ADU, 4}$ occurred exclusively within the decomposition of the ADU powder. The first one underlines the presence of additional H_2O molecules

compared to the IG particles, as suggested by the XRD results. The latter was also recognised during decomposition studies performed on ADU powder [18,20]. Both references assigned it to NH_3 release, Karelin et al. [20] discussed it more in detail and pointed out to several reactions involved in this step (decomposition with release of H_2O and NH_3, adsorption of NH_3 on the formed oxide and partial decomposition of NH_3 into N_2 and H_2).
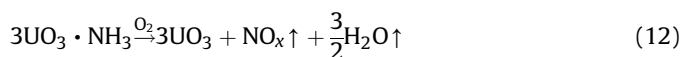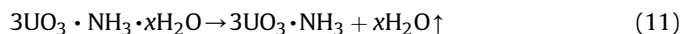
The stoichiometric H_2O and NH_3 coefficients determined are close to the expected values and lead to $\frac{n(H_2O)+n(NH_3)}{n(UO_3)}$ ratios of 1.88 for the IG particles and 2.32 for the ADU powder. Eloirdi et al. [18] proposed a mechanism for the formation of UO_3 from ADU powder, which is based on a HT-XRD study, as well as endothermic and exothermic signals observed in DTA and $\frac{dTGA}{dT}$ data. Taking the atmosphere and stoichiometric coefficients into account, the proposed scheme results in reactions (5) to (7). The educt of reaction (7) was changed from $2UO_3 \cdot NHO_3$ to $2UO_3 \cdot NH_3$, since we assume a typo in the source (Table 1, step 3) [18]. Compound III (Table 3) corresponds to a composition with a NH_3 to UO_3 ratio of $\frac{1}{2}$ and was identified by Eloirdi et al. [18] via XRD for their material. We calculated mass losses normalised to $m(U_3O_8)$ of 0.54 % for reaction (5), 9.09 % for reaction (6) and 3.03 % for reaction (7). The losses of reactions (5) and (6) originate from water release and the loss of reaction (7) from ammonia release. Those theoretical mass differences are included in Table 3 and lead to a total mass loss of 12.66 % for the decomposition of compound III to UO_3.

$$2UO_3 \cdot NH_3 \cdot xH_2O \overset{O_2}{\rightarrow} 2UO_3 \cdot NH_3 \cdot xOH + \frac{x}{2}H_2O\uparrow \tag{5}$$

$$2UO_3 \cdot NH_3 \cdot xOH \rightarrow 2UO_3 \cdot NH_3 + \frac{x}{2}H_2O\uparrow + \frac{x}{4}O_2\uparrow \tag{6}$$

$$2UO_3 \cdot NH_3 \overset{O_2}{\rightarrow} 2UO_3 + NO_x\uparrow + \frac{3}{2}H_2O\uparrow \tag{7}$$

Based on the discussed data we propose a decomposition scheme for the IG particles ($3UO_3 \cdot 2NH_3 \cdot 4H_2O$, compound IV) to UO_3 according to reactions (8) and (9). Note that reaction (9) generalises the NH_3 release observed in the temperature range from 200 °C to 450 °C, but that close inspection of the MS and DSC data (Figs. 6 and 7) may suggest this occurs as two separate steps starting around 200 °C and 350 °C, respectively.

$$3UO_3 \cdot 2NH_3 \cdot 4H_2O \rightarrow 3UO_3 \cdot 2NH_3 + 4H_2O\uparrow \tag{8}$$

$$3UO_3 \cdot 2NH_3 \overset{O_2}{\rightarrow} 3UO_3 + 2NO_x\uparrow + 3H_2O\uparrow \tag{9}$$

For the ADU powder ($3UO_3 \cdot NH_3 \cdot 5H_2O$, compound II), a second reaction step needs to be introduced to account for the removal of additional water molecules (reactions (10) and (11)). The latter can be assigned to a temperature region of 175 °C to 225 °C (Fig. 6). Based on a comparable integral of the first peak for $\frac{m}{z} = 17$ of both materials, we assume a release of about 4 molecules of water within reaction (10) leading to $x = 1$ for reactions (10) and (11). The $\frac{m}{z} = 17$ signal was chosen since the absolute intensity is about one order of magnitudes higher than the one for $\frac{m}{z} = 18$. During the conversion step to β-UO_3 (reaction (9)), a significant lower amount of gaseous material is released compared to the IG particles (reaction (9)). This explains the absence of an additional feature in the MS and DSC data (Figs. 6 and 7) starting around 350 °C, in contrast to results on the IG particles.

$$3UO_3 \cdot NH_3 \cdot 5H_2O \rightarrow 3UO_3 \cdot NH_3 \cdot xH_2O + (5-x)H_2O\uparrow \tag{10}$$

$$3UO_3 \cdot NH_3 \cdot xH_2O \rightarrow 3UO_3 \cdot NH_3 + xH_2O\uparrow \tag{11}$$

$$3UO_3 \cdot NH_3 \overset{O_2}{\rightarrow} 3UO_3 + NO_x\uparrow + \frac{3}{2}H_2O\uparrow \tag{12}$$

The theoretical mass losses for the decomposition of our initial material to UO_3 are 12.60 % for the IG particles (compound IV, Table 3) and 12.72 % for the ADU powder (compound II, Table 3), with NH_3 contributions listed in Table 3. The sum of the losses determined by TGA for the IG particles is 12.88(5) %, which is close to the theoretical mass loss. While for the ADU powder a loss of 14.51(5) % was experimentally measured, supporting the presence of a large amount of adsorbed water which was not removed during the purging prior to the analyses.

Due to the exchange of NH_3 by H_2O, as explained by Cordfunke [17], the discussed data represent a current 'snap-shot' of our material. Moreover, the NH_3 and H_2O fractions might differ for other IG particles or ADU powders, depending on their precipitation conditions ($\frac{n(NH_3)}{n(U)}$) [17].

4.3. Decomposition: formation of UO_3 and conversion to α-U_3O_8

The XRD data reveal the presence of a crystalline β-UO_3 phase in the ADU powder already at 550 °C. However, for the IG particles, a crystalline β-UO_3 phase is not recognised in the HT-XRD pattern (Fig. 2). Similarly, no stable mass plateau was observed for the relevant temperature region in the TGA data (Fig. 5) of the IG particles (102.37(3) % at 500 °C and 102.01(3) % at 580 °C), while for the ADU powder the sample mass does not show a significant variation in the same temperature region (101.94(4) % and 101.86(4) %). Lastly, the lower reaction enthalpy for the transition from UO_3 to α-U_3O_8 (reaction (13)) of the IG particles (72(2) kJ mol^{-1} U_3O_8) compared to the ADU powder (81(2) kJ mol^{-1} U_3O_8) allows to conclude that no pure β-UO_3 phase is formed for the IG particles.

As stated in the Results section, the theoretical mass loss for the conversion of UO_3 to α-U_3O_8 (reaction (13)) corresponds to 1.90 %. The sum of this mass loss and the mass losses for the release of H_2O and NH_3, discussed in the previous subchapter, results in the total mass differences shown in Table 3.

$$3UO_3 \rightarrow U_3O_8 + \frac{1}{2}O_2\uparrow \tag{13}$$

4.4. Decomposition: formation and properties of α-U_3O_8

The crystallisation of α-U_3O_8 follows reaction (13) and started at 550 °C (Fig. 2). At 650 °C the material of both compounds was fully converted to α-U_3O_8. The data are in agreement to HT-XRD studies of Eloirdi et al. [18] who observed the crystallisation of α-U_3O_8 at 600 °C for ADU powder but differ from observations made by Manna et al. [19]. They observed a multiphase region via XRD for ADU powder at temperatures $\leq$ 650 °C, consisting of β-UO_3 and α-U_3O_8, while a treatment temperature of 750 °C resulted in a α-U_3O_8 single phase.

During the α-U_3O_8 formation, we observed along the a axis a decreasing lattice parameter for the IG particles, while the lattice parameter of the ADU powder is constant (Fig. 4a). The trend of the lattice parameter for the a axis was also observed for the b axis, a quite constant value was found for the ADU powder, while the lattice parameter for the IG particles decreased (Fig. 4b). At 650 °C the most significant drop occurred. Along the c axis (Fig. 4c), an expansion was observed for the ADU powder and a contraction for the IG particles. The lattice volume reflects the observations made

for the lattice parameter. The cell volume of the α-U_3O_8 phase formed from the IG particles decreases with increasing temperature (0.3378(4) nm^3, 0.3371(3) nm^3 and 0.3347(2) nm^3), while the cell volume of the α-U_3O_8 phase formed from the ADU powder shows no significant expansion in the considered temperature range (0.3340(2) nm^3, 0.3342(1) nm^3, 0.3343(1) nm^3). The volumes of the α-U_3O_8 phases formed from both materials at 650 °C are quite similar (Fig. 4d) and the XRD pattern of both materials at 650 °C (Fig. 3) match well to the α-U_3O_8 phase (ICSD: 28137 [28]), confirming the formation of a comparable product for both samples. Eloirdi et al. [18] found comparable lattice parameters at 600 °C for α-U_3O_8 produced from ADU powder. The lattice parameters they determined, as well as the cell volume, are included in Fig. 4 and show a good agreement to the data obtained for the ADU powder of this study.

Loopstra [32] determined the *C2mm* space group (non-standard setting of space group *Amm*2) for the α-U_3O_8 phase, following orthorhombic symmetry, with lattice parameters of $a = 0.6716$ nm, $b = 1.1960$ nm and $c = 0.4147$ nm. Our lattice parameters refer to the standard setting in the *Amm*2 space group, resulting in a swap of the *a* with *c* parameter. The values are slightly higher than the ones determined by Loopstra [32], which can be explained by the fact that he recorded the XRD data at room temperature and not *in-situ* via HT-XRD.

5. Conclusion

In this work the thermal decomposition of dried microspheres prepared by the sol-gel method via internal gelation and ammonium diuranate has been investigated in detail by a combination of simultaneous thermal analysis, evolved gas analysis, and non-ambient XRD techniques. Both ADU and the microspheres belong to the $NH_3 - UO_3 - H_2O$ class of materials [17], which differ in NH_3, UO_3 and H_2O contents, but resemble each other closely with respect to crystallographic properties and thermal behaviour. Under the specified preparation conditions, the dried microspheres could be associated to the composition $3UO_3 \cdot 2NH_3 \cdot 4H_2O$, whereas this was $3UO_3 \cdot NH_3 \cdot 5H_2O$ in case of the ADU material, according to XRD. The thermal decomposition of both compounds in air shows distinct reaction steps towards the conversion to α-U_3O_8, in the temperature range between room temperature and 450 °C. Analysis of the mass loss and calorimetric profile, complemented with EGA-MS allowed to derive decomposition schemes, associated to successive release of water and ammonia molecules as temperature increases. Furthermore, HT-XRD demonstrated that the dried microspheres prepared in this study undergo a crystallographic transition via amorphous UO_3 to α-U_3O_8 during thermal decomposition. In contrast, a crystalline β-UO_3 phase is formed as an intermediate product for the ADU powder. This difference may be associated to the prolonged release of NH_3 in the microspheres, due to the higher $\frac{NH_3}{H_2O}$ ratio compared to ADU. Finally, at temperatures above 550 °C both compounds are transformed into α-U_3O_8, which becomes slightly hypostoichiometric at high temperatures. New insights in the thermal decomposition process of the compounds $3UO_3 \cdot 2NH_3 \cdot 4H_2O$ and $3UO_3 \cdot NH_3 \cdot 5H_2O$ were obtained, which, combined with recent results on the compound $2UO_3 \cdot NH_3 \cdot 3H_2O$ using a similar methodology [18], complete our understanding of the $NH_3 - UO_3 - H_2O$ class of materials originally described by Cordfunke [17] in 1962.

Data availability statement

The data required to reproduce these findings are available to download from the repository *zenodo* [25].

Declaration of competing interest

The authors declare that they have no known competing financial interests or personal relationships that could have appeared to influence the work reported in this paper.

References

[1] F.W. Van Der Brugghen, M.E.A. Hermans, J.B.W. Kanij, A.J. Noothout, T. Van Der Plas, H.S.G. Slooten, Sol-gel Processes for the Preparation of Spherical Thorium-Containing Fuel Particles, Technical Report, Keuring van Electrotechnische Materialen, NV, Arnhem (Netherlands), 1968.

[2] R. Förthmann, Die chemischen Grundlagen des Hydrolyseverfahrens zur Herstellung sphärischer Kernbrennstoffteilchen, Technical Report Jül-950-RW, Kernforschungsanlage Jülich, Institut für Reaktorwerkstoffe, 1973.

[3] P.A. Haas, J.M. Begovich, A.D. Ryon, J.S. Vavruska, Chemical flowsheet conditions for preparing urania spheres by internal gelation, Ind. Eng. Chem. Prod. Res. Dev. 19 (1980) 459—467, https://doi.org/10.1021/i360075a033.

[4] R.D. Hunt, J.L. Collins, Uranium kernel formation via internal gelation, Radiochim. Acta 92 (2004) 909—915, https://doi.org/10.1524/ract.92.12.909.55110.

[5] V.N. Vaidya, Status of sol-gel process for nuclear fuels, J. Sol. Gel Sci. Technol. 46 (2008) 369—381, https://doi.org/10.1007/s10971-008-1725-0.

[6] S. Li, J. Bai, S. Cao, X. Yin, C. Tan, P. Li, W. Tian, J. Wang, H. Guo, Z. Qin, An improved internal gelation process without cooling the solution for preparing uranium dioxide ceramic microspheres, Ceram. Int. 44 (2018) 2524—2528, https://doi.org/10.1016/j.ceramint.2017.11.001.

[7] M.A. Pouchon, G. Ledergerber, F. Ingold, K. Bakker, Sphere-pac and VIPAC fuel, in: R.J. Konings (Ed.), Comprehensive Nuclear Materials, Elsevier BV, Oxford, 2012, pp. 275—312, https://doi.org/10.1016/b978-0-08-056033-5.00059-8.

[8] S. Suryanarayana, N. Kumar, Y.R. Bamankar, V.N. Vaidya, D.D. Sood, Fabrication of UO$_2$pellets by gel pelletization technique without addition of carbon as pore former, J. Nucl. Mater. 230 (1996) 140—147, https://doi.org/10.1016/0022-3115(96)00162-6.

[9] A. Kumar, J. Radhakrishna, N. Kumar, R.V. Pai, J.V. Dehadrai, A.C. Deb, S.K. Mukerjee, Studies on preparation of (U$_{0.47}$,Pu$_{0.53}$)O$_2$ microspheres by internal gelation process, J. Nucl. Mater. 434 (2013) 162—169, https://doi.org/10.1016/j.jnucmat.2012.11.009.

[10] G. Ledergerber, F. Ingold, R.W. Stratton, H.-P. Alder, C. Prunier, D. Warin, M. Bauer, Preparation of transuranium fuel and target materials for the transmutation of actinides by gel coconversion, Nucl. Technol. 114 (1996) 194—204, https://doi.org/10.13182/NT96-A35249.

[11] H. Daniels, Herstellung uranbasierter Keramiken mittels interner Gelierung zur Konversion trivalenter Actinoiden, Ph.D. thesis, RWTH Aachen, 2012, https://juser.fz-juelich.de/record/22866.

[12] C. Schreinemachers, A.A. Bukaemskiy, M. Klinkenberg, S. Neumeier, G. Modolo, D. Bosbach, Characterization of uranium neodymium oxide microspheres synthesized by internal gelation, Prog. Nucl. Energy 72 (2014) 17—21, https://doi.org/10.1016/j.pnucene.2013.07.016.

[13] V.N. Vaidya, S.K. Mukerjee, J.K. Joshi, R.V. Kamat, D.D. Sood, A study of chemical parameters of the internal gelation based sol-gel process for uranium dioxide, J. Nucl. Mater. 148 (1987) 324—331, https://doi.org/10.1016/0022-3115(87)90026-2.

[14] J.L. Collins, M.F. Lloyd, R.L. Fellows, The basic chemistry involved in the internal-gelation method of precipitating uranium as determined by pH measurements, Radiochim. Acta 42 (1987) 121—134, https://doi.org/10.1524/ract.1987.42.3.121.

[15] M.H. Lloyd, K. Bischoff, K. Peng, H.-U. Nissen, R. Wessicken, Crystal habit and phase attribution of U(VI) oxides in a gelation process, J. Inorg. Nucl. Chem. 38 (1976) 1141—1147, https://doi.org/10.1016/0022-1902(76)80237-0.

[16] A.S. Abdel-Halim, F.A. El-Nour, N. Belacy, H.F. Aly, T. Khalil, Physico-chemical characteristics of uranium oxide microspheres produced by internal gelation, Isotopenpraxis Isotopes in Environmental and Health Studies 26 (1990) 524—529, https://doi.org/10.1080/10256019008622420.

[17] E.H.P. Cordfunke, On the uranates of ammonium − I: the ternary system NH$_3$−UO$_3$−H$_2$O, J. Inorg. Nucl. Chem. 24 (1962) 303—307, https://doi.org/10.1016/0022-1902(62)80184-5.

[18] R. Eloirdi, D. Ho Mer Lin, K. Mayer, R. Caciuffo, T. Fanghänel, Investigation of ammonium diuranate calcination with high-temperature X-ray diffraction,

J. Mater. Sci. 49 (2014) 8436—8443, https://doi.org/10.1007/s10853-014-8553-0.

[19] S. Manna, P. Karthik, A. Mukherjee, J. Banerjee, S.B. Roy, J.B. Joshi, Study of calcinations of ammonium diuranate at different temperatures, J. Nucl. Mater. 426 (2012) 229—232, https://doi.org/10.1016/j.jnucmat.2012.03.035.

[20] A.I. Karelin, A.N. Zhiganov, O.P. Lobas, A.A. Zhiganova, Mechanism and kinetics of thermal-decomposition of ammonium uranates in various gaseous media, Radiokhimiya 31 (1989) 117—124.

[21] P.A. Haas, J.M. Begovich, A.D. Ryon, J.S. Vavruska, Chemical Flowsheet Conditions for Preparing Urania Spheres by Internal Gelation, Technical Report ORNL/TM-6850, Oak Ridge National Laboratory (ORNL), 1979, https://doi.org/10.2172/6104596.

[22] I. Grenthe, J. Drożdżyński, T. Fujino, E.C. Buck, T.E. Albrecht-Schmitt, S.F. Wolf, Uranium, in: L.R. Morss, N.M. Edelstein, J. Fuger (Eds.), The Chemistry of the Actinide and Transactinide Elements, Springer Netherlands, Dordrecht, 2011, pp. 253—698, https://doi.org/10.1007/978-94-007-0211-0_5.

[23] R.D. Hunt, J.L. Collins, M.H. Lloyd, S.C. Finkeldei, Production of more ideal uranium trioxide microspheres for the sol-gel microsphere pelletization process without the use of carbon, J. Nucl. Mater. 515 (2019) 107—110, https://doi.org/10.1016/j.jnucmat.2018.12.029.

[24] J. Härtwig, G. Hölzer, E. Förster, K. Goetz, K. Wokulska, J. Wolf, Remeasurement of characteristic X-ray emission lines and their application to line profile analysis and lattice parameter determination, Phys. Status Solidi 143 (1994) 23—34, https://doi.org/10.1002/pssa.2211430104.

[25] C. Schreinemachers, G. Leinders, Thermal Decomposition Data of Uranium Containing Microspheres Produced via Internal Gelation and Ammonium Diuranate Powder, 2019, https://doi.org/10.5281/zenodo.3250894 (license: CC BY-NC-SA).

[26] L.J. Cabri, J.H.G. Laflamme, Rhodium, platinum, and gold alloys from the Stillwater Complex, Can. Mineral. 12 (1974) 399—403. https://pubs.geoscienceworld.org/canmin/article-pdf/12/6/399/3419701/399.pdf.

[27] P.C. Debets, B.O. Loopstra, On the uranates of ammonium — II: X-ray investigation of the compounds in the system $NH_3-UO_3-H_2O$, J. Inorg. Nucl. Chem. 25 (1963) 945—953, https://doi.org/10.1016/0022-1902(63)80027-5.

[28] B.O. Loopstra, On the existence of δ-U_3O_8; a comment on papers by Karkhanavalla and George, and by Amirthalingam, J. Nucl. Mater. 29 (1969) 354—355, https://doi.org/10.1016/0022-3115(69)90214-1.

[29] C. Guéneau, A. Chartier, L.V. Brutzel, Thermodynamic and thermophysical properties of the actinide oxides, in: R.J. Konings (Ed.), Comprehensive Nuclear Materials, Elsevier, Oxford, 2012, pp. 21—59, https://doi.org/10.1016/B978-0-08-056033-5.00009-4.

[30] M.C. Burrell, D.A. Lee, Analysis of UO_3 gel Microsphere Decomposition Products by Mass Spectrometry, Technical Report ORNL/TM-6649, Oak Ridge National Laboratory (ORNL), 1979, https://doi.org/10.2172/6358824.

[31] D.A. Lee, D.P. Stinton, Evaluation of Urania Gel Pyrolysis by Mass Spectrometry, Technical Report ORNL/TM-6538, Oak Ridge National Laboratory (ORNL), 1978, https://doi.org/10.2172/6537976.

[32] B.O. Loopstra, The structure of β-U_3O_8, Acta Crystallogr. B 26 (1970) 656—657, https://doi.org/10.1107/S0567740870002935.